ACSNANO

www.acsnano.org

ARTICLE

Power Backpack for Energy Harvesting and Reduced Load Impact

Ze Yang,[⊥] Yiyong Yang,[⊥] Fan Liu, Zhaozheng Wang, Yinbo Li, Jiahao Qiu, Xuan Xiao, Zhiwei Li, Yijia Lu, Linhong Ji, Zhong Lin Wang,* and Jia Cheng*

Cite This: https://dx.doi.org/10.1021/acsnano.0c07498

Read Online

ACCESS | Metrics & More | Article Recommendations | Supporting Information

ABSTRACT: Long-distance walking with heavy loads is often needed when going hiking or for field rescue, which is prone to cumulative fatigue. There is also a great need for labor-saving and biomechanical energy harvesting in daily life for extended security and communication needs. Here, we report a load-suspended backpack for harvesting the wasted energy of human motion based on a triboelectric nanogenerator (TENG). Two elastomers are incorporated into the backpack to decouple the synchronous movement of the load and the human body, which results in little or no extra accelerative force. With such a design, through theoretical analysis and field experiments, the backpack can realize a reduction of 28.75 % in the vertical oscillation of the load and 21.08 % in the vertical force on the wearer, respectively. Meanwhile, the mechanical-to-electric energy conversion efficiency is modeled and calculated to be 14.02 % under normal walking conditions. The designed backpack has the merits of labor-saving and shock absorption as well as electricity generation, which has the promising potential to be a power source for small-scale wearable and portable electronics, GPS systems, and other self-powered health care sensors.

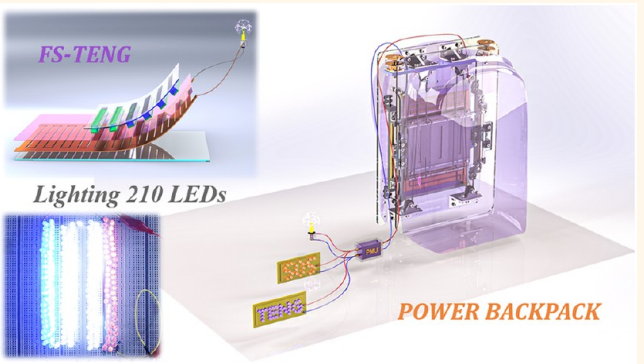

KEYWORDS: *backpack, triboelectric nanogenerator, labor-saving, shock absorption, energy harvesting*

Backpacks are widely used in our daily life, giving tremendous freedom to the hands and serving as a great convenience for life and production.[1−4] There are many tough situations where walking or running with heavy loads[5] in a backpack is demanded, such as field training, outdoor hiking, fire-fighting rescue, *etc.* It is of great necessity and extreme importance to continuously provide electricity for the increasingly used portable and wearable electronics and sensors on people[6−9] such as athletes, explorers, disaster rescuers, *etc.*, who work in wild or rural areas.

Moreover, considering the fact that batteries such as Li-ion batteries have a limited lifetime and stored electricity,[10,11] much effort has been devoted to seeking a sustainable, renewable, and environmentally friendly complement to establish self-powered systems.[12−14] For instance, harvesting energy from mechanical movements or vibrations in the environment is a good choice.[15−17] Meanwhile, human motions such as walking, running, breathing, and heart and pulse beating all have the potential to be energy sources.[18−21] To effectively use the wasted mechanical energy of human movements, many energy harvesters[22−25] based on piezoelectric,[26−31] electromagnetic,[32−35] and electrostatic induction[36,37] effects have been recently developed to harvest biomechanical energies from the foot strike, ankle, knee, elbow, and hip.[20,38] Among them, it is efficient and important to generate electricity from the up and down movements of the mass center of human body during walking or running.[20]

The triboelectric nanogenerator (TENG),[39−42] as a method of harvesting ambient energy, has been created and exploited. It is based on the coupling of the electrostatic induction effect and the triboelectrification effect.[43−45] Since being created in 2012 by Wang *et al.*,[46] it has witnessed rapid developments and great achievements in the self-powered sensors,[47−52] micro-nano energies,[23,53−55] blue-ocean energies,[56−59] and high voltage applications.[60−64] The TENG has shown many advantages in converting mechanical energy into electrical

Received: September 5, 2020
Accepted: January 14, 2021

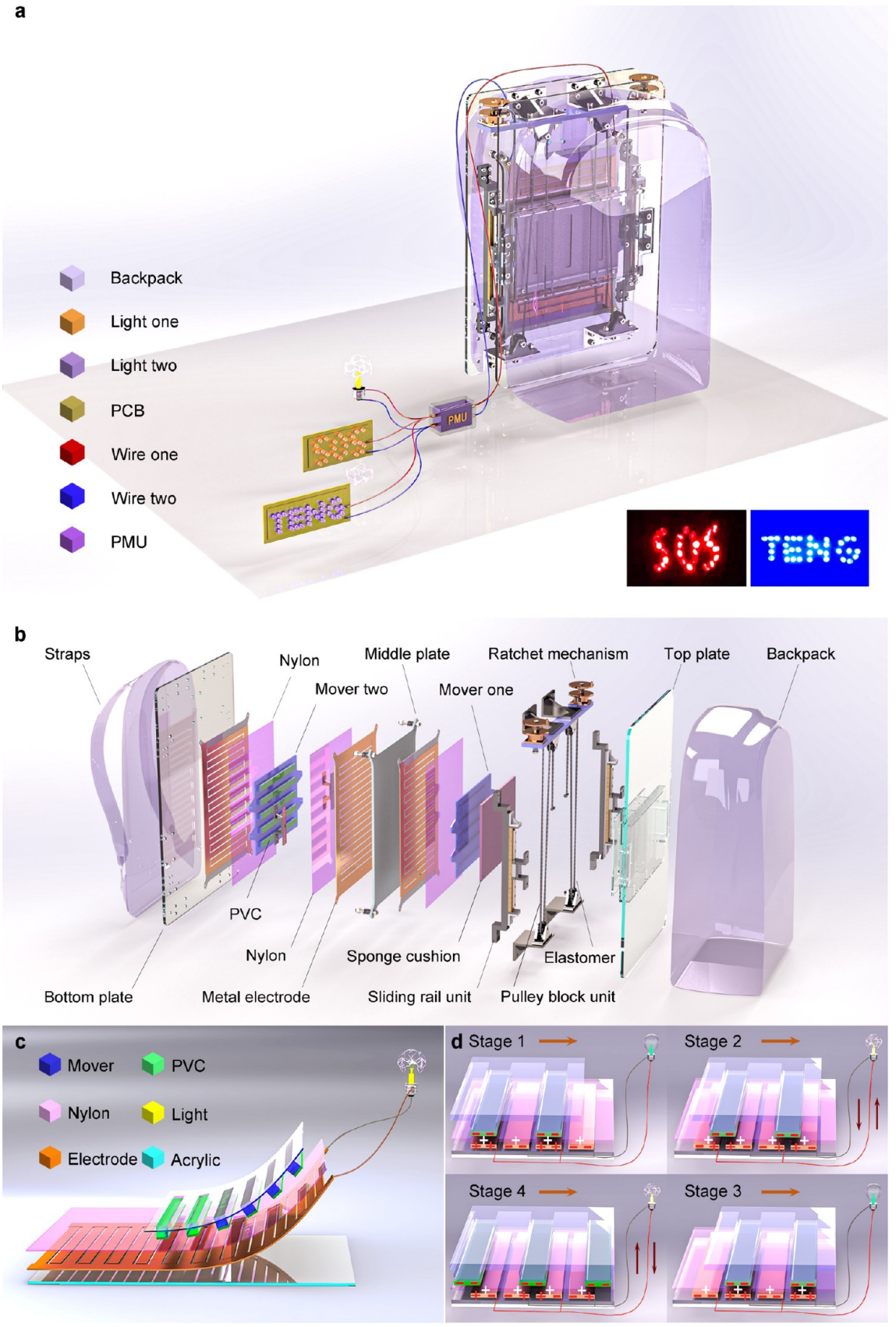

Figure 1. Structural and schematic photographs of the load-suspended backpack. (a) Schematic diagram of the whole backpack. Under the unlocked condition, alternating currents generated can power some lower powered electronic products through a power management unit (PMU). (b) Structural illustration of the backpack in the explosion state without presenting fasteners. (c) Schematic diagram of the TENG. It adapts the IDT electrode and there are some grating rows on the movers. (d) Schematics of the four stages in an electric cycle, and the reversal of electric polarity leads to an alternating current in the circuit.

https://dx.doi.org/10.1021/acsnano.0c07498
ACS Nano XXXX, XXX, XXX−XXX

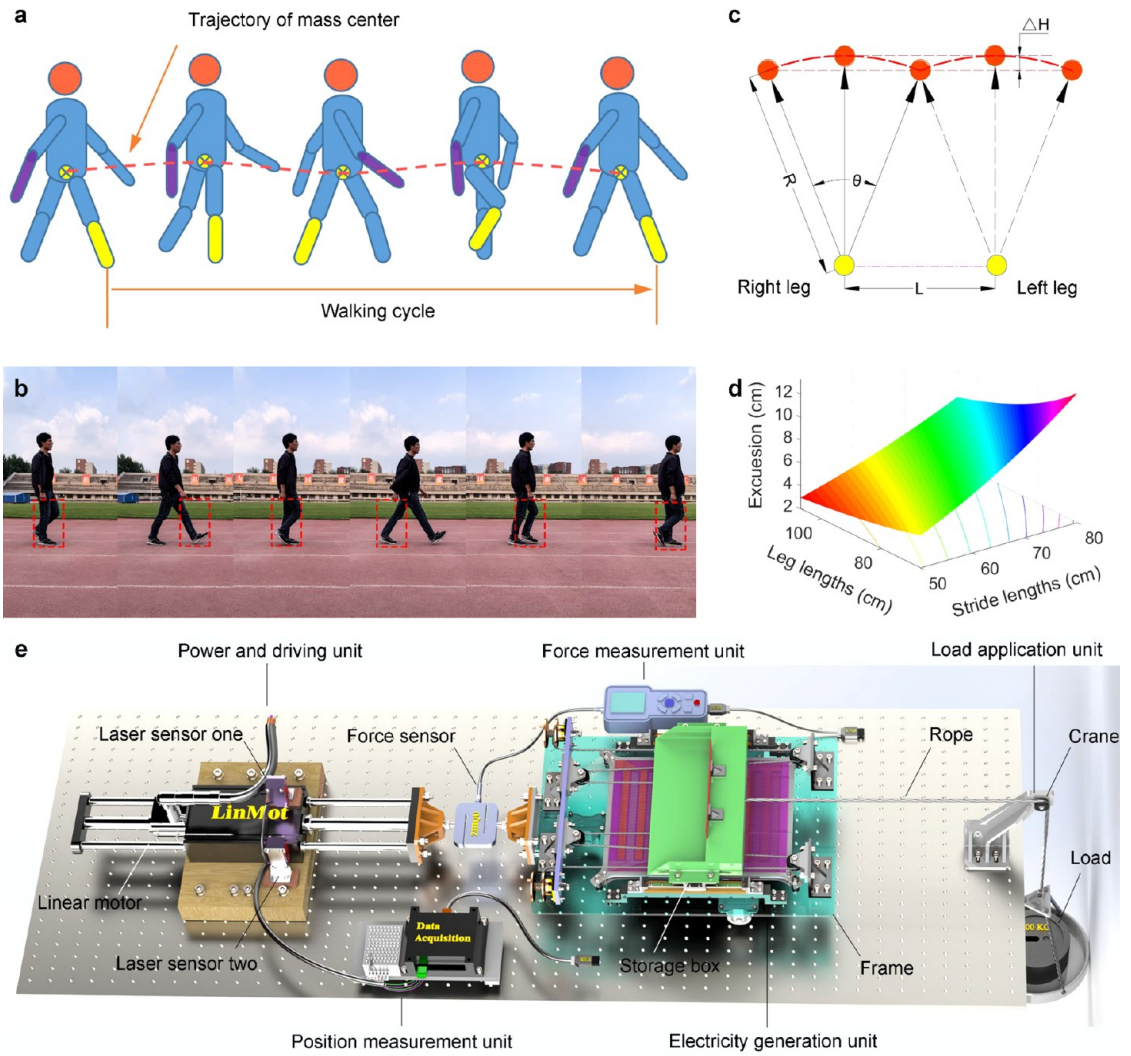

Figure 2. Gait analysis and the equivalent experiment system. (a) Motion postures of the walking. The red dotted line is the trajectory of the body's mass center in a walking cycle. (b) Gait motion in one walking cycle under actual environment. The postures of the left leg in the red dotted boxes refer to a whole walking cycle. (c) Double inverted pendulum as the mode of walking, approximately simplified from the lower extremity. In this model, the mass center of the human body traces out two arcs with a vertical excursion (ΔH) and R, L, and θ are the leg length, stride length, and span angle, respectively. (d) Relationship map of the vertical excursion with the leg length and the stride length. (e) Scheme of the equivalent experiment system with a counterpart vehicle shouldering a load-suspended box. The system consists of five sections including power and driving unit, force measurement unit, load application unit, position measurement unit, and electricity generation unit.

energy under a low-frequency environment, such as high output power, high energy conversion efficiency, low cost, and easy fabrication.[29,65,66] In the literature, there are a few applications of TENG to harvest the mechanical energy in a backpack. Yang *et al.*[67] developed a backpack embedded with a rationally designed TENG with integrated rhombic gridding in order to harvest vertical vibration energy through the contact and separation of two materials. This backpack was characterized by its structural form and high energy conversion efficiency. Another work comes from Chandrasekhar *et al.*,[68] who developed a smart backpack using a triboelectric nanogenerator to collect biomechanical energy from different human motions including walking, running, and bending. However, those backpacks approximately adopted the contact-separation mode of TENG with a relatively low power output, and in particular, they all lack the capacity of labor-saving and shock absorption.

The electromagnetic generator (EMG), as a traditional generator, is based on electromagnetic induction and is widely used to provide clean electricity. As reported in previous literature,[69−71] there are some works incorporating the EMG into a backpack. However, considering their limitations of complexity and heavy weight, we explore a method of adopting the TENG to harvest the energy of walking and running, which is more suitable to the ambient atmosphere with lower frequencies.[56]

Human walking can be regarded as an inverted pendulum, where the hip joint traces up an arc over the leg with a vertical excursion of 5−7 cm.[69,72,73] The conventional backpack falls into step with the body due to their fixed connection, resulting in an extra accelerative force on the wearer. Hereby, we reported a load-suspended backpack for energy harvesting based on TENG (LSBP-TENG). Two elastomers were used to decouple the synchronous movement of the human body and backpack. This made the labor-saving and shock absorption

https://dx.doi.org/10.1021/acsnano.0c07498
ACS Nano XXXX, XXX, XXX−XXX

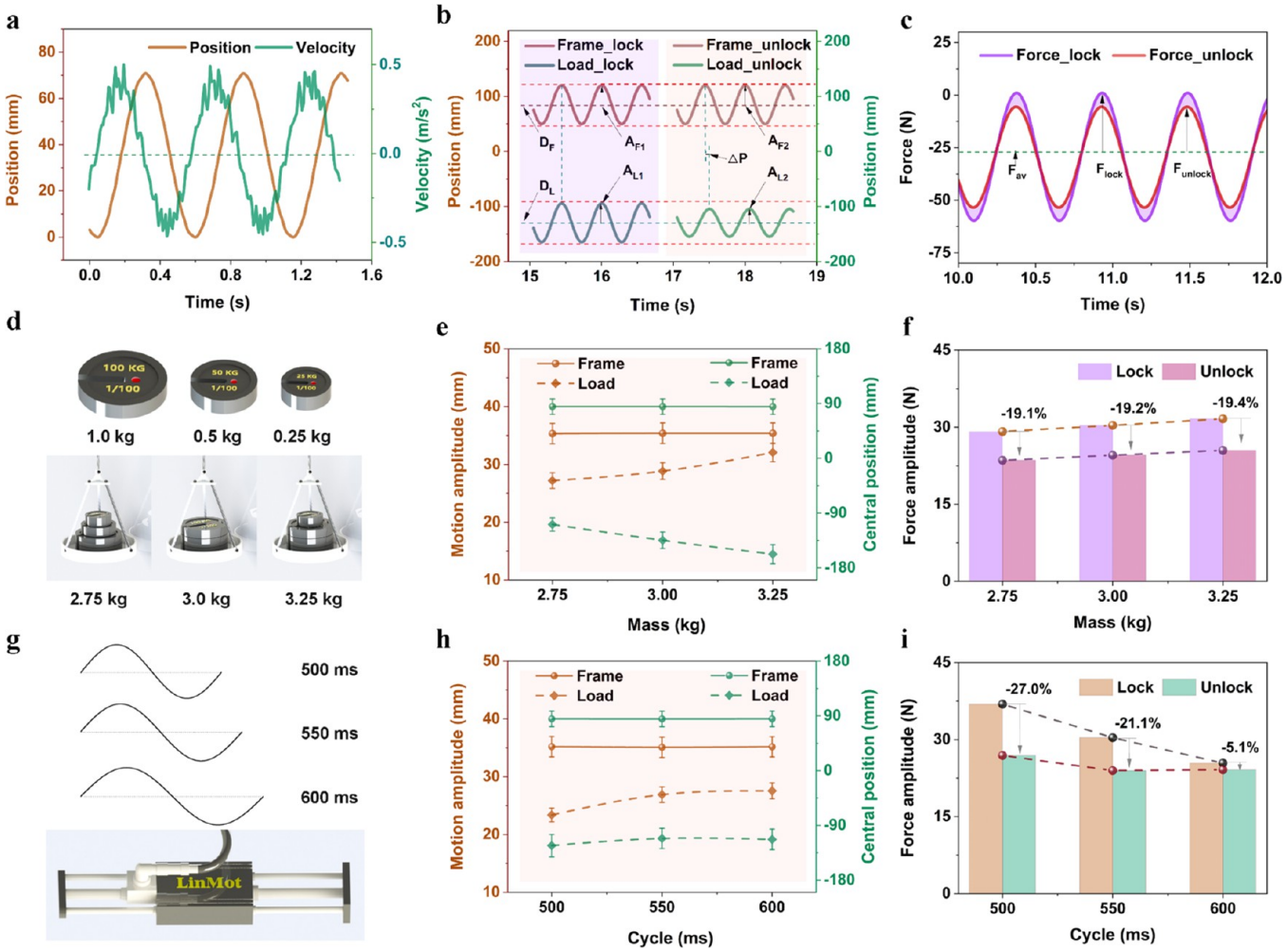

Figure 3. Position and force of the backpack under different driving frequencies and applied loads. (a) Driving motion provided by the linear motor. (b) Positions of the backpack under the locked and unlocked conditions. (c) Driving forces under the locked and unlocked conditions. (d) Different loads stored in the salver. (e) Motion amplitudes (A_{F2}, A_{L2}) and central positions (D_F, D_L) of the load and frame with different loads. (f) Amplitudes of the driving forces with different loads. (g) Different gait cycles provided by the linear motor. (h) Motion amplitudes (A_{F2}, A_{L2}) and central positions (D_F, D_L) of the load and frame with different gait cycles. (i) Amplitudes of the driving forces with different gait cycles.

possible. In addition, there was a relative motion between the load and the backpack, which directly drove the TENG. Through the theoretical calculations and field experiments, the LSBP-TENG realized a reduction of 28.75 % in vertical oscillation and 21.08 % in accelerative vertical force, respectively. Meanwhile, the peak power density was up to 58.82 W/m^2 and the final energy conversion efficiency was 14.02 % under the normal walking condition. This LSBP-TENG can not only help the wearer to carry with a heavier load but also has the promising potential to be an energy source for the small-scale wearable electric devices, which is beneficial to children, field scientists, athletes, and others who wear a backpack.

RESULTS AND DISCUSSION

Structural Design of the Load-Suspended Backpack. The structure of this LSBP-TENG and the schematic diagrams of its working principle are illustrated in Figure 1 and video S1. There are two restrained conditions: locked condition and unlocked condition. The LSBP-TENG is rigidly connected with the human body under the locked condition, similar to traditional backpacks. Under the unlocked condition, the synchronous movement of the backpack and human body is decoupled through the stretch and shrink of two embedded elastomers. At the same time, the relative motion between the load and the backpack drives the triboelectric nanogenerator (TENG) for mechanical-to-electric energy conversion. Hereby, the generated alternating current can be rectified to power some electric apparatuses like the lower-powered lamp and the commercial light-emitting diodes (LEDs) through a power management unit (PMU) (Figure 1a). The insets at the right bottom of Figure 1a are photographs of lighted diodes directly driven by TENG.

As shown in Figure 1b, the two movers, the cushion and the top plate, are fixed together with bolt connections, and the two terminal ends of one elastomer are fastened to the top plate and the ratchet mechanism through the pulley blocks, respectively. Under the gravity of loads, the two elastomers are stretched and the top plate moves up and down on two linear slide rails during walking, as shown in Figure S1.

Meanwhile, the two movers synchronously move with the top plate. Then this synchronous motion directly drives the TENG for electricity generation. In addition, the ratchet

https://dx.doi.org/10.1021/acsnano.0c07498
ACS Nano XXXX, XXX, XXX−XXX

mechanism is used to adjust the tension of elastomers by clockwise or anticlockwise rotation of the ratchet heads.

There are some polyvinyl chloride (PVC) films in a square shape on grating rows of two movers, and the nylon films are attached to the surfaces of three copper IDT electrodes. Driven by the top plate, the PVC films slide on the nylon films and the alternating current is produced to power a lower-powered lamp (Figure 1c).

The working principle of electricity generation is based on TENG (Figure 1d), and the first and third electrodes are connected together as electrode E_1, the second and fourth electrodes as electrode E_2 from the left to right view direction. The PVC films fully contact with the electrode E_1. Since the PVC is more triboelectrically negative than nylon,[74,75] the negative charges occur on the PVC films and the positive ones on the nylon films with an equal amount. Meanwhile, owing to the electrostatic induction effect, positive charges are induced on the electrode E_1 underneath while negative ones in equal quantity on the electrode E_2 (stage 1). The PVC films then start to slide rightward and reach the middle position, and an induced electric potential drop between electrode E_1 and E_2 drives electrons flowing from electrode E_2 to electrode E_1 through an external load, resulting in an electric equilibrium (stage 2). Then the PVC films continuously slide rightward and the flowing of electrons also continues. When they fully contact with the electrode E_2, there is an inverse charge distribution against the first stage (stage 3). Finally, a reversed current occurs in the circuit with the continuous rightward sliding of PVC films, resulting in another electric equilibrium similar to stage 2 (stage 4). Hence, the TENG serves as an electron pump to drive electrons flowing back and forth between two electrodes E_1 and E_2, which generates an alternating current in the circuit.[45,61,62] Notably, an inverse process will occur if the PVC films slide leftward.

Gait Analysis and Equivalent Experimental System. Normal walking is made up of four movement phases including foot contacting the ground, leg supporting the body, leg being lifted, and leg swing, and moreover, the trajectory of the mass center of the body is a double arc in the entire walking cycle, as shown in Figure 2a. The actual leg postures in the red boxes in Figure 2b illustrate the motion pattern in Figure 2a.

To discover the relationship of the vertical excursion with the stride length and the leg length, a double arc model of walking is established, as depicted in Figure 2c. The leg length, stride length, vertical excursion, and span angle are symbolized by R, L, ΔH, and θ, respectively. Through the detailed derivation in Supporting Note S1, the vertical excursion (ΔH) is the function of leg length (R) and stride length (L). Moreover, it increases with the stride length and the decrease of leg length, as illustrated in Figure 2d.

When walking at a normal speed of 4.7 km/h, the vertical excursion was calculated to be 6.98 cm and the step frequency was 1.82 Hz (550 ms/cycle) on average (Figure S2 and Table S1). This meets with the reported ranges of 5−7 cm and 1.58−2.08 Hz.[73] To accurately perform the single-factor experiment, an equivalent experiment system is established, as shown in Figure 2e and the Figure S3. The system is made up of five units: the power and driving unit for providing precise movement by a magneto-electric linear motor, the force measurement unit for obtaining the driving force by a force sensor located between the linear motor and the vehicle, the load application unit, the position measurement unit for observing the displacements of the load and the frame by two laser sensors, and the electricity generation unit based on TENG. This experiment system can ensure a precise input of motion parameters with the linear motor. The position and velocity of the motor are triggered and controlled by the red-dotted cosine curves in Figure 2c. Consequently, the vertical excursion and step frequency of walking are substituted by the displacement and move frequency of the linear motor.

Analysis of the Motion and Force. The LSBP-TENG mostly works in the unlocked condition. It is necessary to discover the relationships between the labor-saving and vibration absorption with the walking speeds and the loads. With the obtained walking parameters and the structural constraint of this backpack, the experimental walking frequencies are 1.67, 1.82 and 2.00 Hz (600, 550, 500 ms/cycle) and the three different loads are 2.75, 3.00, and 3.25 kg.

With the maximum driving displacement of 6.98 cm (the vertical excursion) and an oscillation frequency of 1.82 Hz (550 ms/cycle), the linear motor moves according to the position and velocity curves in Figure 3a. Moreover, as illustrated in the left purple part of Figure 3b, the absolute displacement of load had the same amplitude value (A_{F1} = 35.111 mm) and motion phase ($\Delta P = 0°$) as that of the frame (A_{L1} = 35.111 mm) under the locked condition. But the load obtained a smaller motion amplitude (A_{L2} = 25.015 mm) and a slower motion phase (ΔP = 35.54°) than that of the frame (A_{F2} = 35.111 mm) under the unlocked condition. In other words, it was reduced by 28.75 % in the oscillation amplitude, as shown in the right orange part of Figure 3b.

In addition, the labor saving of this LSBP-TENG is evaluated by the difference of driving forces under the locked and unlocked conditions. When taking a load of 3.00 kg, as shown in Figure 3c, the driving force under the unlocked condition had a smaller amplitude than that under the locked condition ($F_{unlock} < F_{lock}$), and it was reduced by 21.08 % (from 30.367 to 23.967 N). Therefore, there is a labor-saving and shock absorption in our designed backpack.

When taking different loads (Figure 3d) with a constant gait cycle (550 ms), the motion amplitudes (A_{F2}, A_{L2} in Figure 3b) and the central position (D_F, D_L in Figure 3b) are collected in Figure 3e. Obviously, the A_{L2} (the dotted orange line in Figure 3e) increases with the loads, while the relative motion ($\Delta A = A_{F2} - A_{L2}$, the difference between the solid orange line and the dotted orange line in Figure 3e) decreases with the loads. Meanwhile, the D_L (the dotted green line in Figure 3e) and the relative distance ($\Delta D = D_F - D_L$, the difference between the solid green line and the dotted green line in Figure 3e) both increase with the loads (minus sign only reflects the inverse direction). In addition, as shown in Figure 3f, the force amplitudes (F_{lock} and F_{unlock} in Figure 3c, $F_{lock} > F_{unlock}$) both increase with the loads under two conditions (Figure 3f) and the difference between them ($\Delta F = F_{lock} - F_{unlock}$) remains nearly unchanged (about 19.2 %) (Figure 3f and Figure S4).

When walking at different gait cycles (Figure 3g) with the same load (3.0 kg), as shown in Figure 3h, the A_{L2} increases with the gait cycles while the ΔA decreases with the gait cycles. Meanwhile, the D_L and ΔD nearly stay unchanged. In addition, as shown in Figure 3i, the force amplitudes (F_{lock} and F_{unlock} in Figure 3c, $F_{lock} > F_{unlock}$) both decrease with the gait cycles under two conditions and so does the difference between them (from 27.0 % to 5.1 %) (Figure S5).

In other words, the faster the walking speed is, the lighter the load will feel and the greater the labor-saving will be. We can conclude that the load and the walking speed both play an

https://dx.doi.org/10.1021/acsnano.0c07498
ACS Nano XXXX, XXX, XXX−XXX

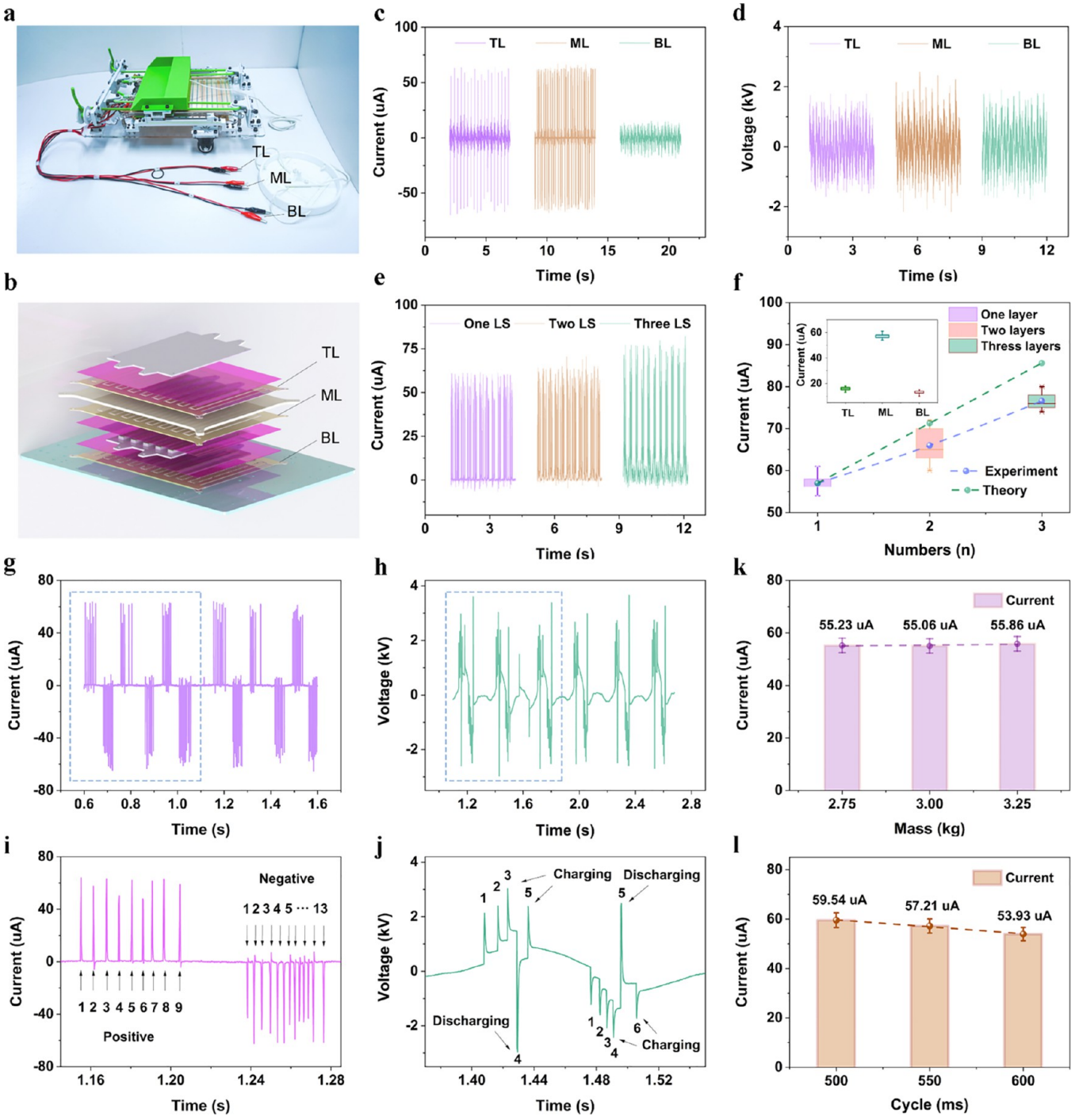

Figure 4. Electrical measurements of the electricity generation based on TENG. (a) Photograph of the counterpart vehicle in the experiment. (b) Structure of the TENG in the counterpart vehicle. (c, d) Open-circuit voltage and short-circuit current of different layers including the top layer (TL), middle layer (ML), and bottom layer (BL) with the TENG in the freestanding triboelectric-layer mode. (e) Rectified short-circuit currents of one, two, and three layers of TENGs. (f) Difference between the average currents under the field experiment and theoretical summation. The inset is the current from a single layer of TENG. (g, h) Polarities of the current and voltage alternately changing with the time. The current or voltage beams in the dotted box occur within one motion cycle. (i, j) Two current beams and two voltage beams with one time of polarity change. There is a charging and discharging phenomenon during the process. (k, l) Short-circuit currents under the different loads or gait cycles.

important role in the labor-saving and vibration absorption, while the latter takes up a larger share.

Characteristics of the Generated Electricity. The multilayer structure is employed to enhance the current output. The output current theoretically increases with the amounts of layers, while three layers (n = 3) of IDT electrodes are finally adopted considering the carrying comfortability and the weight.

As shown in Figure 4a,b, the counterpart vehicle in the experiment has three layers of IDT electrodes for TENG including the top layer (TL), the middle layer (ML), and the bottom layer (BL). The generated electricity is extracted out

https://dx.doi.org/10.1021/acsnano.0c07498
ACS Nano XXXX, XXX, XXX−XXX

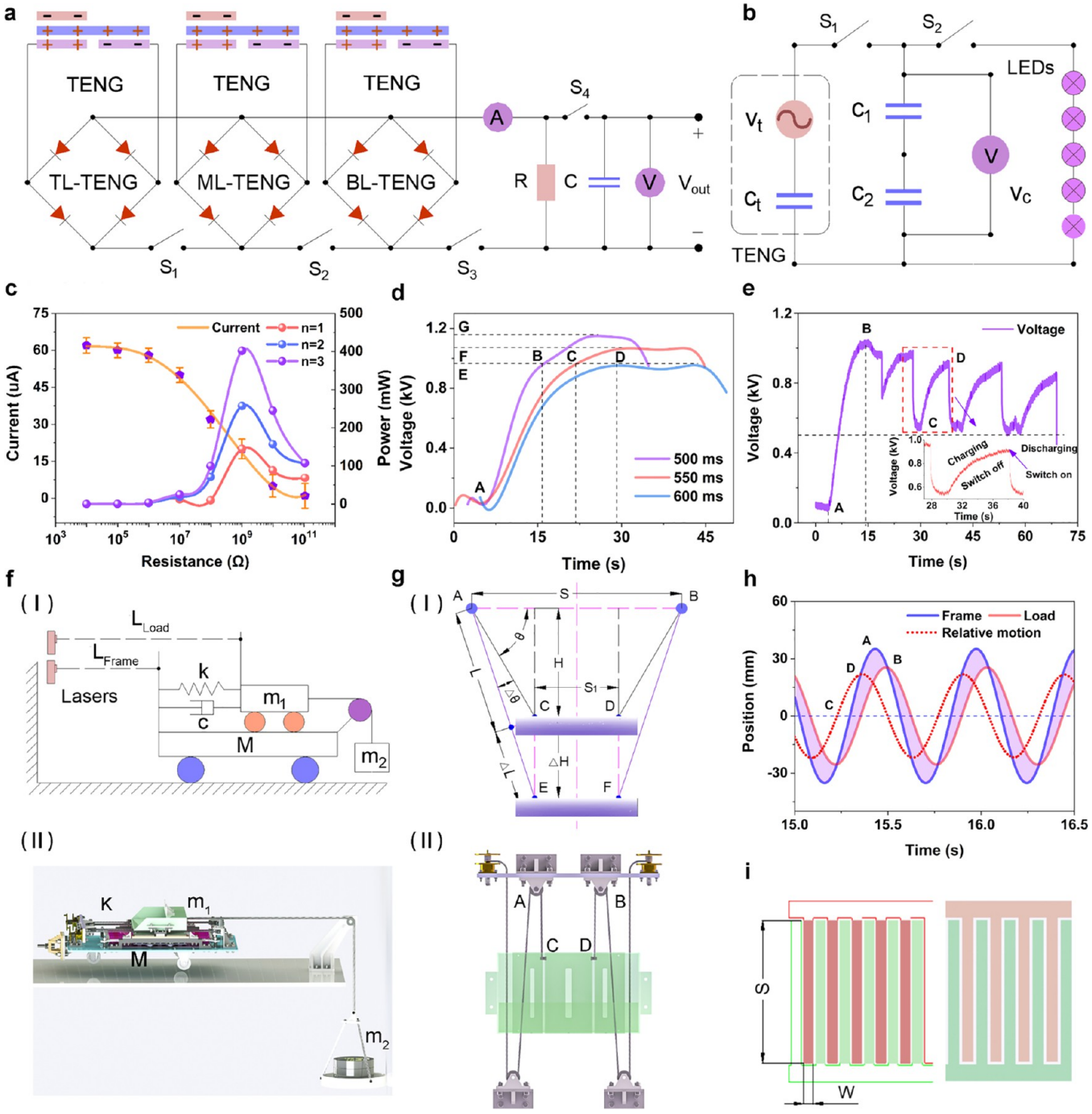

Figure 5. Electric power output and mechanical-to-electric energy conversion efficiency. (a) Systematic electric circuit for the electricity output. (b) Circuit model of a single layer of TENG, used for the following capacitor experiment. (c) Current curve on different external resistances from one layer of TENG (n = 1) and the peak power curves under various external loads for TENGs with n = 1, 2, and 3. (d) Charging time for a high voltage ceramic capacitor (22 nF, 3 kV/223). (e) Charging and then discharging curves of a ceramic capacitor. The LEDs are lit with the switch on (point D) and the voltage simultaneously goes down, as shown in the enlarged view of the inset. (f) Theoretical mode for the calculation of conversion efficiency of energy (I) and the partial structure of experiment system (II). (g) Analytical mode (I) for obtaining the extension (ΔL) of the elastomer and the partial structure of elastomer and pulley blocks (II). The relative movement between the load and frame is constrained between the point C and point E (ΔH). (h) Relative motion of the load to frame, equal to the displacement of frame subtracts that of the load. (i) Single-deck IDT electrode used in the design. The partial rectangle bars of it simultaneously participate in the process of electricity generation.

through three current channels. Measured by an electrometer (Keithley 6514), as shown in Figure 4c,d, the short-circuit currents and the open-circuit voltages are 58 μA and 1.3 kV for the top layer, 60 μA and 1.5 kV for the middle layer, 15 μA and 1.2 kV for the bottom layer. In comparison, the differences among the currents or voltages (Figure 4c,d) originate from different contact status between two material films. Furthermore, the currents are more sensitive to the contact states than the voltages owing to the larger difference among the currents than the voltages.

https://dx.doi.org/10.1021/acsnano.0c07498
ACS Nano XXXX, XXX, XXX−XXX

Moreover, when simultaneously connected with different number of layers, the open-circuit peak currents after being rectified become 60 μA for n = 1, 65 μA for n = 2, and 75 μA for n = 3 (Figure 4e). Moreover, the average currents from field experiments have lower amplitudes than that from the theoretical summation for n = 2, 3 (Figure 4f). Their difference is on the decrease with the number of layers, implying a small destructive interaction in the electricity output. The inset in Figure 4f reports the output currents from different layers.

In addition, observing the curves in Figure 4c,d with a small-scale view, the grating structure determines an alternating electric polarity between two electrodes and the currents and voltages are reversed three times in a gait cycle, as seen in the boxes in Figure 4g,h.

Observing the curves in Figure 4g,h with a smaller scale view, there are 9 positive current peaks and 13 negative ones in a gait cycle (Figure 4i) and 5 positive voltage peaks and 6 negative ones (Figure 4j). According to the polarity change of the left fourth voltage peak and the right fifth one in Figure 4j, the first charging and later discharging phenomenon take place both in the positive and negative phases, which may be attributed to the narrow gully between two grating electrodes. The current or voltage peaks are of difference in amount and in impulse form before and after the change of electric polarity, which can be related to the different intensity and times of contacts between two material films.

Meanwhile, as seen in Figure S6, the output current in parallel connection has a higher amplitude than that in serial, while their output voltages are approximately the same. Therefore, the parallel connection of the three layers of electrodes is preferred to get a better output. Similarly, when taking different loads, the output current of one layer almost remains 55 μA (Figure 4k) but decreases with the gait cycles (Figure 4l). In other words, the loads have little effect on the electricity output, but the faster walking speeds lead to greater electricity output.

Electric Power and Energy Conversion Efficiency. A conversion circuit including some diodes, switches, resistors, and capacitors is established to transform the alternating current (AC) of TENGs into direct current (DC) (Figure 5a). Three rectifier bridges are respectively assigned to the top layer (TL), the middle layer (ML), and the bottom layer (BL), conducting the full-wave rectifications. As depicted in Figure 5b, the TENG can be regarded as an energy source with high voltage and a capacitor with high impedance in series connection, and the generated electricity can be stored in the capacitors and then is used to power the LEDs. This simplified circuit is to be used for charging the following experimental capacitors. The output current decreases with the external loads due to the Ohmic loss (current curve in Figure 5c) and the maximum instantaneous peak powers are located at the load resistance of 1 GΩ when n = 1, 2, and 3 (power curves in Figure 5c).

Furthermore, the shorter time is demanded to charge a high voltage ceramic capacitor (22 nF, 3 kV/223) for reaching the same voltage when taking a faster driving speed ($t_B < t_C < t_D$) (Figure 5d). Meanwhile, the faster driving speed also leads to a higher utmost voltage ($V_G > V_F > V_E$) (Figure 5d). The voltage curve of this capacitor in Figure 5d is then drawn with several times of charging and discharging processes, which shows the charging speed is fast at the early stage but slows down with the time going on (Figure 5e and the inset). The charging process starts from the point A and ends with a saturated voltage at the point B, then the discharging is performed with the switch on. For example, the capacitor is charged again at point C and discharged at point D when turning the switch on; meanwhile, the voltage immediately slashes down.

From the view of energy conversion, the mechanical-to-electric energy conversion efficiency $\eta_{electric}$ is defined as the ratio of output electric energy to the vibration energy in the unlocked backpack. To complete this calculation, a simplified vibration mode with single degree of freedom is proposed to explore the relationship between the motion and energy, as shown in Figure 5f. The upper picture (I) in Figure 5f is simplified from part of experiment system (the lower picture (II) in Figure 5f), as an equivalent vibration mode.

Based on the conservation law of energy, the decreased gravitational potential energy ($E_{gravity}$) of the load (m_2) is divided into three parts including the elastic potential energy ($E_{elastic}$) stored in elastomers, the output electric energy ($E_{electric}$), and the wasted thermal energy ($E_{thermal}$) by the friction effect, expressed as eq 1.

$$E_{gravity} = E_{elastic} + E_{electric} + E_{thermal} \tag{1}$$

When the load descends a distance (ΔH) at an even speed in the vertical direction, the extension (ΔL) of the elastomer occurs along with the movement of the load. In order to disclose the relationship between ΔL and ΔH, a simplified geometric mode of the elastomer and pulley block unit is established (Figure 5g), in which the ΔH is detailly illustrated in the Figure S7. The upper picture (I) in Figure 5g is simplified from the structure of elastomer and pulley blocks (the lower picture (II) in Figure 5g), as an equivalent theoretical mode. The ΔL is to be used for the following calculation of the electric energy ($E_{electric}$), and it has the same type of motion but a slightly smaller amplitude than the ΔH, as seen in Figure S8a. In addition, the relative motion has a lower oscillation amplitude ($D_a < B_a < A_a$) but an earlier motion phase ($D_p > A_p > B_p$) than that of the load of the frame (Figure 5h). The load, the frame, and their relative motion have the same gait cycle.

Owing to the small deformation effect, the elastomer with a small extension length can be regarded as the spring with a constant stiffness. On the basis of Hooke's law and work principle, the elastic potential energy can be estimated as eq 2

$$E_{elastic} = \frac{1}{2} K_{equal} \Delta L^2 \tag{2}$$

where the stiffness of elastomer K_{equal} is 992.43 N/m, which is equal to half of the maximum and minimum stiffness when the elastomer is stretched longest and shortest (Figure S8b,c). The ΔL is 42.72 mm as described in Supporting Note S2. Moreover, the gravitational potential energy and electric energy can be described as eqs 3 and 4

$$E_{gravity} = M_{load} g \Delta H \tag{3}$$

$$E_{electric} = Q = N \int_{t_1}^{t_2} I^2 R \, dt \tag{4}$$

where ΔH is 42.94 mm, the masses of load with the tray and rope M_{load} are 4 kg, and the acceleration of gravity g is 9.8 N/kg. Q is Joule heating energy, N is 3, I is the instantaneous current, and R is the load resistance of maximum output mentioned above. The beginning time t_1 and the end time t_2 are 90.8 and 362.7 ms, respectively. The $E_{electric}$ is consequently 117.99 mJ based on the above parameters.

https://dx.doi.org/10.1021/acsnano.0c07498
ACS Nano XXXX, XXX, XXX−XXX

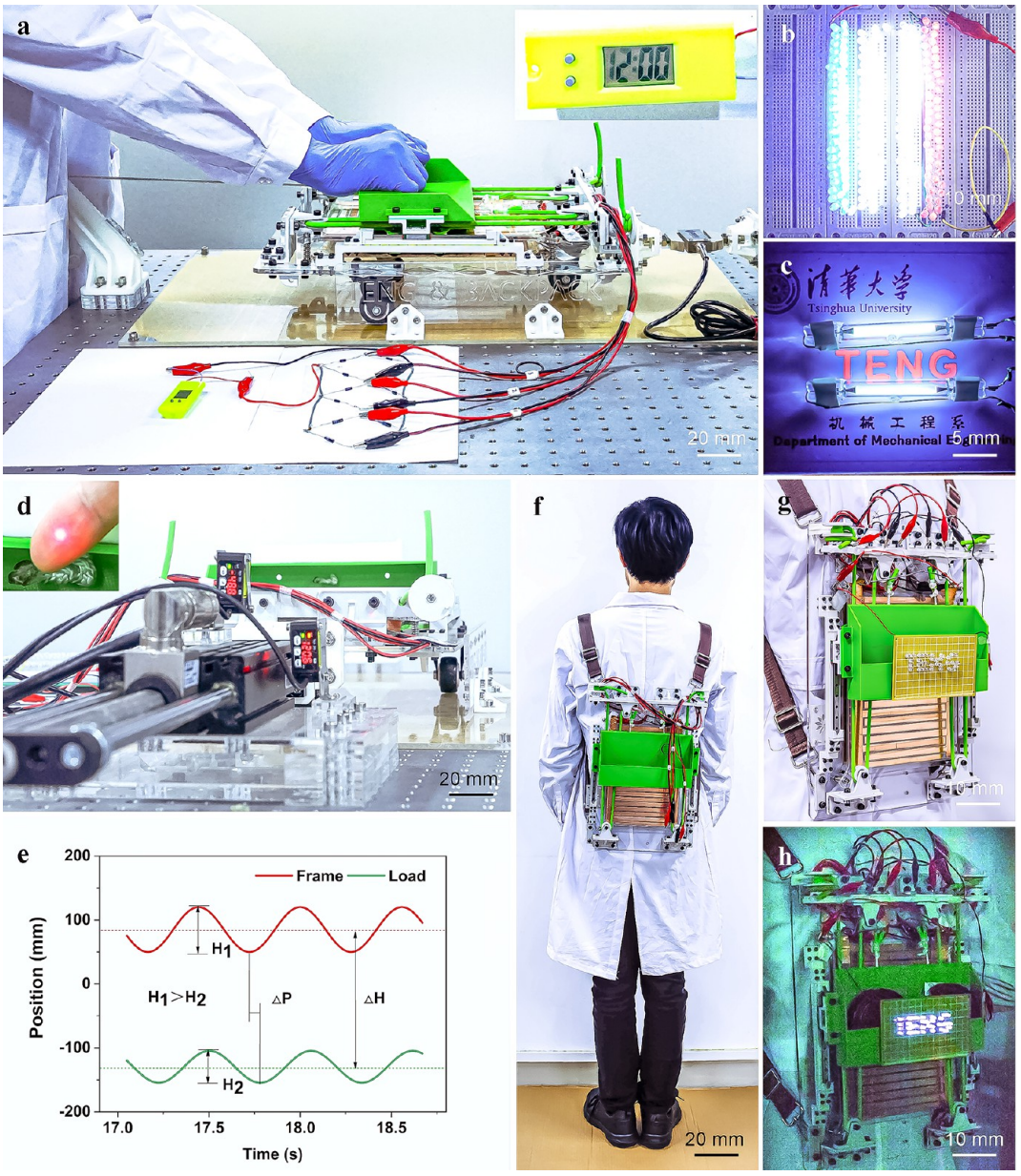

Figure 6. Application and field experiment of the device. (a) Experimental device driven by the hands or the linear motor. The inset at the top right corner is the photograph of a low-wattage electric watch. (b) Photograph of 210 lighted LEDs in array when being powered by TENG. (c) Photograph of two lighted ultraviolet tubes in series. They are used for the visualization of fluorescent ink, suggesting a relatively high voltage. (d) Photograph of two laser sensors for obtaining the absolute displacements of load and frame. The inset at the top left corner is an image of the red laser beam shining on a finger. (e) Graph of the absolute positions of the load and frame. (f) Photograph of the simplified prototype, and the electricity is extracted outside through three circuit pathways. (g) Experimental photographs on the treadmill without the load. (h) Experimental photographs on the treadmill with the load. The copyright of the logo of Tsinghua University (THU) belongs to THU. The use of the logo in this publication is permitted.

Since there is no loss in $E_{electric}$ but the $E_{thermal}$ is depleted, the $\eta_{electric}$ and $\rho_{electric}$ are the efficiency of energy conversion and the instantaneous power density, respectively, calculated as eqs 5 and 6

$$\eta_{electric} = \frac{E_{electric}}{E_{gravity} - E_{elastic}} \times 100 \quad (5)$$

$$\rho_{electric} = \frac{E_{electric}}{S_{electric}\Delta t} = \frac{E_{electric}}{NSW(t_2 - t_1)} \quad (6)$$

where $S_{electric}$ is the total working area simultaneously participating in the electricity generation. The mover simultaneously contacts with five bars of the electrode every time (Figure 5i), resulting in that the number of working grating rows of electrode N is 5 and the length S and width W of each row are 147.5 and 10 mm, respectively (Figure 5i). Consequently, the efficiency of energy conversion is 14.02 %, and the instantaneous power density is 58.82 W/m^2. Accordingly, the LSBP-TENG is a promising energy harvester to power some low-powered electronics by harvesting the vibration energy during the walking.

https://dx.doi.org/10.1021/acsnano.0c07498
ACS Nano XXXX, XXX, XXX−XXX

Application and Field Experiment of the Device. As shown in Figure 6a, the alternating current is generated by the relative motion between the load and the frame. Then it is rectified to power the LEDs, the electric watch, the ultraviolet tubes, and so on. The inset in Figure 6a is a photograph of an electric watch powered by TENG. Driven by human hands with a little endeavor, the produced current is high enough to simultaneously light 210 LEDs or more (Figure 6b and video S2) and the output voltage is high enough to power two ultraviolet tubes in series for the visualization of font "TENG" printed with fluorescent ink on a specially designed label (Figure 6c and video S3).

In addition, the relative motion of the load and frame is measured by two laser sensors, as shown in Figure 6d. And the static values of the upper and lower sensors are the original locations of them, used to calculate the extension of elastomer. The inset in Figure 6d is an image of a red laser beam shining on a finger. As shown in Figure 6e, the load has a smaller motion amplitude than that of the frame ($H_2 < H_1$) and a slower motion phase (ΔP) as well as an initial gap spacing to the frame (ΔH). These results demonstrated the possibility and rationality of the structure design. As shown in Figure 6f, the simplified backpack has the similar structure as the one in Figure 1a, the electricity is extracted outside through three circuit pathways, and the storage box is used to store the applied loads.

When walking without the load, the storage box stays at the top location without any relative movement to the frame (Figure 6g). When walking with the load, the elastomer is stretched and the storage box moves to the middle location with the equal opportunity of moving up and down to generate electricity. As shown in Figure 6h and the video S4, the LEDs are lit when the user walks on a treadmill with the load, and the faster walking speed will result in a brighter shining of LEDs.

On the basis of the load suspension technology and triboelectric nanogenerator, the LSBP-TENG has three merits including the labor-saving, shock absorption and electricity generation. Two elastomers are applied to decouple the synchronous motion between the load and the backpack's frame, resulting in relative motion for generating electricity. The increases of loads and walking speed both contribute to the labor-saving and shock absorption. Moreover, a fatigue test is performed to evaluate the fatigue resistance of two materials, as shown in Figures S9 and S10 and video S5.

However, there is still an upside potential in the performance with a better structural organization such as adopting the longer sliding rails to elongate the relative motion in the next generation. Meanwhile, the energy conversion efficiency can be improved with much effort such as improving the stiffness of elastomer for heavier loads, optimizing the structure of metal electrodes, adopting the nanomaterial modification of two contact materials, and taking the hybridization of electromagnetic mode, *etc.* Lastly, the problem of mass production should be faced and solved with further efforts as well as the challenges of the standardization of structure parts, the simplicity of function units, custom-tailored production, and ergonomics, *etc.*

Further study may focus on how to enhance its performance with the mentioned methods above and the practical problem of mass production. The LSBP-TENG has a wide range of applications such as relieving the load burden on school children, allowing rescuers to carry more and heavier equipment, providing continuous electrical energy for wearable and portable electrics, GPS systems, and other self-powered health care sensors, and so on.

CONCLUSIONS

We have reported the design and working principle of a load-suspended backpack for energy harvesting based on the triboelectric nanogenerator (LSBP-TENG), which can realize labor savings and oscillation absorption as well as electricity generation. The synchronous motion between the load and the frame of backpack is decoupled by the stretch and shrink of two elastomers, resulting in a relative motion for generating electricity. There is a reduction of 28.75 % in the vertical oscillation and a 21.08 % in the labor-saving. Meanwhile, the produced short-circuit current and open-circuit voltage of a single layer of electrode are 60 μA and 1.5 kV, respectively, which are high enough to light the lower-powered electronic watch, 210 LEDs and two ultraviolet tubes. Through the theoretical calculation, the peak power density is 58.82 W/m^2 and the energy conversion efficiency is 14.02 %. In conclusion, the LSBP-TENG can enable heavier loads than the traditional ones under the same condition and has the promising potential to be an energy source for the wearable and portable electrics and sensors.

METHODS AND MATERIALS

Fabrication of the Backpack Based on TENG. The major components of the LSBP-TENG are installed on a rectangular acrylic plate of 420 mm in length, 300 mm in width, and 5 mm in thickness, which is fabricated by a laser cutter (version CM-1309, G.U. Eagle America, Inc., USA). There are several through holes made by laser boring on the bottom plate, and they are used for the fixation of components with bolts. Two commonly used linear sliding rails and blocks in the same type are symmetrically fixed on two sides of the bottom plate, and the sliding rail has a length of 128 mm and an install height of 35 mm to the surface of the bottom plate. There are three layers of electrode slices, one of which is on the bottom plate, the other two are distributed on two sides of the middle plate. The middle plate is fixed on the bottom plate with four compression springs and four long bolts.

The electrode slice is made as follows: first, a sinuous groove is sculptured on a rectangle acrylic plate of 232 × 185 × 2 mm with four prominent ears for fixation; second, a rectangle copper film of 0.065 mm in thickness is covered on the acrylic plate; third, the copper film is cut away to form two groups of separate grating copper electrode; finally, the nylon film of 0.025 mm in thickness is adhered onto the copper electrode. The two movers with grating rows in the array are made by the fused deposition modeling (FDM) of 3D printing with acrylonitrile butadiene styrene (ABS) material on a printer (version 3DP-25-4F, Tiertime, Inc., China). Located among the electrode slices, the two movers are fixed together to synchronously move up and down with the top plate. Most of the components are fabricated by 3D printing with ABS materials.

Measurement of Driving Force and Absolute Displacement. The driving force in the experiment system is equivalently regarded as the force on the shoulders of wearers, offered by a linear motor (version P01-37 × 120-C/C1100, LinMot, Inc., USA). A force measurement system (version AD2016SC2, AutoDA, Inc., China) with a sensor in "Z" shape is employed, which can display in real time the fluctuation of force on a LCD screen. The force sensor of 70 × 60 × 10 mm is suspended between the linear motor and the vehicle through two connectors. Meanwhile, the locations of the load and the frame are measured by two laser sensors (version HG-C1400, Panasonic, Inc., Japan). And a data acquisition collector is used for real-timely monitoring and recording the motion datum.

Measurement of the Output Electricity. The polarities of the short-circuit current and open-circuit voltage alternately change with time, and they are measured by a Keithley 6514 system electrometer

https://dx.doi.org/10.1021/acsnano.0c07498
ACS Nano XXXX, XXX, XXX−XXX

(Keithley 6514, impedance >200 TΩ, Keithley, Inc., USA). Moreover, a high voltage ceramic capacitor (22 nF, 3 kV/223) is charged to be saturated by the TENG and is then discharged by five LEDs in series. During this process, the Keithley 6514 system electrometer is used to real-timely obtain the voltage changes between two terminals of capacitors with a high-voltage probe (version HVP-40, 1/1000, Pintech, Inc., China). Finally, the still-shot images of some commercial LEDs and two lighted ultraviolet tubes both come from a digital camera (version ILCE-7M2, Sony, Inc., Japan).

ASSOCIATED CONTENT

Supporting Information

The Supporting Information is available free of charge at https://pubs.acs.org/doi/10.1021/acsnano.0c07498.

Structural description of the different partial components in the backpack; gait cycle and stride length under several parallel tests; photograph of the experiment system on an optical platform; driving forces measured with different loads; driving forces measured with different gait cycles; currents and voltages in the parallel and series connections; schematic diagram for measuring the relative displacement between the load and frame; parameters for the calculation of energy conversion efficiency; fatigue test of two materials driven by the linear motor; fatigue features of the materials after fatigue test; raw datum of the gait cycles and stride lengths; calculation of the vertical excursion during the walking; calculation of the stretch length of elastomers (PDF)

Video S1: Structural description of the designed backpack (MP4)

Video S2: Description of the experiment process powered by the linear motor and hands (MP4)

Video S3: The output voltage is high enough to light up the ultraviolet tubes for the visualization of fluorescent ink (MP4)

Video S4: Display of the relative motion and generated electricity when walking or running on a treadmill (MP4)

Video S5: Fatigue experiment of the used materials to obtain their fatigue feature (MP4)

Raw data for the important curves (XLSX)

AUTHOR INFORMATION

Corresponding Authors

Zhong Lin Wang − *Beijing Institute of Nanoenergy and Nanosystems, Chinese Academy of Sciences, Beijing 100083, China; School of Materials Science and Engineering, Georgia Institute of Technology, Atlanta, Georgia 30332-0245, United States;* orcid.org/0000-0002-5530-0380; Email: zhong.wang@mse.gatech.edu

Jia Cheng − *State Key Laboratory of Tribology, Department of Mechanical Engineering, Tsinghua University, Beijing 100084, China;* orcid.org/0000-0002-2557-0072; Email: chengjia@tsinghua.edu.cn

Authors

Ze Yang − *State Key Laboratory of Tribology, Department of Mechanical Engineering, Tsinghua University, Beijing 100084, China; School of Engineering and Technology, China University of Geosciences (Beijing), Beijing 100083, China;* orcid.org/0000-0002-2062-7367

Yiyong Yang − *School of Engineering and Technology, China University of Geosciences (Beijing), Beijing 100083, China*

Fan Liu − *State Key Laboratory of Tribology, Department of Mechanical Engineering, Tsinghua University, Beijing 100084, China;* orcid.org/0000-0001-6586-3307

Zhaozheng Wang − *State Key Laboratory of Tribology, Department of Mechanical Engineering, Tsinghua University, Beijing 100084, China*

Yinbo Li − *State Key Laboratory of Tribology, Department of Mechanical Engineering, Tsinghua University, Beijing 100084, China*

Jiahao Qiu − *State Key Laboratory of Tribology, Department of Mechanical Engineering, Tsinghua University, Beijing 100084, China*

Xuan Xiao − *State Key Laboratory of Tribology, Department of Mechanical Engineering, Tsinghua University, Beijing 100084, China*

Zhiwei Li − *State Key Laboratory of Tribology, Department of Mechanical Engineering, Tsinghua University, Beijing 100084, China*

Yijia Lu − *State Key Laboratory of Tribology, Department of Mechanical Engineering, Tsinghua University, Beijing 100084, China*

Linhong Ji − *State Key Laboratory of Tribology, Department of Mechanical Engineering, Tsinghua University, Beijing 100084, China*

Complete contact information is available at: https://pubs.acs.org/10.1021/acsnano.0c07498

Author Contributions

⊥Z.Y. and Y.Y. contributed equally to this work.

Author Contributions

Z.Y., J.C., and Z.W. conceived the idea and guided the project. Z.Y., Y.Y., and J.C. were in charge of the overall design and fabrication of the backpack, experiments, data recording, and analysis. F.L., Z.W., Y.L., and Y.L. contributed with ideas for the experimental designs and assisted with the measurement of mechanical and electrical characteristics. J.Q., X.X., and Z.L. assisted with the fabrication of the backpack and the video records of experimental results. L.J. contributed to the design of the entire experimental scheme, the data processing, and the description of results. All the authors discussed the results and prepared the manuscript.

Notes

The authors declare no competing financial interest.

The data that supports the plots within this paper and the other findings of this study are available from the corresponding authors upon reasonable request.

ACKNOWLEDGMENTS

This work was supported by the National Natural Science Foundation of China (No. 52075286, U1613207), the National Science and Technology Major Project of China (No. 2011ZX02403), the National Key Research and Development Program of China (No. 2018YFF0300606), and the Tsinghua University Initiative Scientific Research Program (No. 20193080001).

REFERENCES

(1) Barbosa, J. P.; Marques, M. C.; Neiva, H. P.; Esteves, D.; Izquierdo, M.; Alvarez, C.; Marinho, D. A. Effects of Backpacks on Ground Reaction Forces in Children of Different Ages When

https://dx.doi.org/10.1021/acsnano.0c07498
ACS Nano XXXX, XXX, XXX−XXX

Walking, Running, and Jumping. *Int. J. Environ. Res. Public Health* **2019**, *16*, 5154.
(2) Presta, V.; Galuppo, L.; Mirandola, P.; Galli, D.; Pozzi, G.; Zoni, R.; Capici, S.; Colucci, M. E.; Veronesi, L.; Ambrosini, L.; Gobbi, G.; Vitale, M.; Pasquarella, C. One-Shoulder Carrying School Backpack Strongly Affects Gait Swing Phase and Pelvic Tilt: A Case Study. *Acta Biol. Med. Ger.* **2020**, *91*, 168−170.
(3) Connolly, B.; Cook, B.; Hunter, S.; Laughter, M.; Mills, A.; Nordtvedt, N.; Bush, A. Effects of Backpack Carriage on Gait Parameters in Children. *Pediatr. Phys. Ther.* **2008**, *20*, 347−355.
(4) Ahmad, H. N.; Barbosa, T. M. The Effects of Backpack Carriage on Gait Kinematics and Kinetics of School Children. *Sci. Rep.* **2019**, *9*, 1−6.
(5) Cui, X. J.; Cao, S. L.; Guo, R.; Khan, S. A.; Xie, G.; Tian, Z. G.; Sang, S. B.; Zhang, H. L. Building Self-Powered Emergency Electronics Based on Hybrid Nanogenerators for Field Survival/Rescue. *Energy Sci. Eng.* **2020**, *8*, 574−581.
(6) Cao, Y. Printed Wearable Lithium-Ion Electrodes with High Electrochemical Performance as Portable Batteries. *J. Mater. Sci.* **2020**, *55*, 8241−8250.
(7) Zhang, Z.; Zhang, J.; Zhang, H.; Wang, H.; Hu, Z.; Xuan, W.; Dong, S.; Luo, J. A Portable Triboelectric Nanogenerator for Real-Time Respiration Monitoring. *Nanoscale Res. Lett.* **2019**, *14*, 1−11.
(8) Seung, W.; Gupta, M. K.; Lee, K. Y.; Shin, K. S.; Lee, J. H.; Kim, T. Y.; Kim, S.; Lin, J.; Kim, J. H.; Kim, S. W. Nanopatterned Textile-Based Wearable Triboelectric Nanogenerator. *ACS Nano* **2015**, *9*, 3501−3509.
(9) Tu, J.; Torrente, R. M.; Wang, M.; Gao, W. The Era of Digital Health: A Review of Portable and Wearable Affinity Biosensors. *Adv. Funct. Mater.* **2020**, *30*, 1906713.
(10) Ryu, H.; Yoon, H. J.; Kim, S. W. Hybrid Energy Harvesters: Toward Sustainable Energy Harvesting. *Adv. Mater.* **2019**, *31*, 1802898.
(11) Tan, P.; Zheng, Q.; Zou, Y.; Shi, B.; Jiang, D.; Qu, X.; Ouyang, H.; Zhao, C.; Cao, Y.; Fan, Y. A Battery-Like Self-Charge Universal Module for Motional Energy Harvest. *Adv. Energy Mater.* **2019**, *9*, 1901875.
(12) Guo, H.; Yeh, M.-H.; Lai, Y.-C.; Zi, Y.; Wu, C.; Wen, Z.; Hu, C.; Wang, Z. L. All-in-One Shape-Adaptive Self-Charging Power Package for Wearable Electronics. *ACS Nano* **2016**, *10*, 10580−10588.
(13) Ray, P. Renewable Energy and Sustainability. *Clean Technol. Environ. Policy* **2019**, *21*, 1517−1533.
(14) Luo, J.; Wang, Z. L. Recent Advances in Triboelectric Nanogenerator Based Self-Charging Power Systems. *Energy Storage Mater.* **2019**, *23*, 617−628.
(15) Zhang, H.; Wang, H.; Zhang, J.; Zhang, Z.; Yu, Y.; Luo, J.; Dong, S. A Novel Rhombic-Shaped Paper-Based Triboelectric Nanogenerator for Harvesting Energy from Environmental Vibration. *Sens. Actuators, A* **2020**, *302*, 111806.
(16) Tian, J.; Chen, X.; Wang, Z. L. Environmental Energy Harvesting Based on Triboelectric Nanogenerators. *Nanotechnology* **2020**, *31*, 242001.
(17) Yin, M.; Lu, X.; Qiao, G.; Xu, Y.; Wang, Y.; Cheng, T.; Wang, Z. L. Mechanical Regulation Triboelectric Nanogenerator with Controllable Output Performance for Random Energy Harvesting. *Adv. Energy Mater.* **2020**, *10*, 2000627.
(18) Kim, D. H.; Shin, H. J.; Lee, H.; Jeong, C. K.; Park, H.; Hwang, G. T.; Lee, H. Y.; Joe, D. J.; Han, J. H.; Lee, S. H. *In Vivo* Self-Powered Wireless Transmission Using Biocompatible Flexible Energy Harvesters. *Adv. Funct. Mater.* **2017**, *27*, 1700341.
(19) Proto, A.; Penhaker, M.; Conforto, S.; Schmid, M. Nanogenerators for Human Body Energy Harvesting. *Trends Biotechnol.* **2017**, *35*, 610−624.
(20) Choi, Y.-M.; Lee, M. G.; Jeon, Y. Wearable Biomechanical Energy Harvesting Technologies. *Energies* **2017**, *10*, 1483.
(21) Park, D. Y.; Joe, D. J.; Kim, D. H.; Park, H.; Han, J. H.; Jeong, C. K.; Park, H.; Park, J. G.; Joung, B.; Lee, K. J. Self-Powered Real-Time Arterial Pulse Monitoring Using Ultrathin Epidermal Piezoelectric Sensors. *Adv. Mater.* **2017**, *29*, 1702308.
(22) Martin, J.-P.; Li, Q. Design, Model, and Performance Evaluation of a Biomechanical Energy Harvesting Backpack. *Mech. Syst. Sig. Process.* **2019**, *134*, 106318.
(23) Lin, Z. M.; Wu, Y. F.; He, Q.; Sun, C. C.; Fan, E. D.; Zhou, Z. H.; Liu, M. Y.; Wei, W.; Yang, J. An Airtight-Cavity-Structural Triboelectric Nanogenerator-Based Insole for High Performance Biomechanical Energy Harvesting. *Nanoscale* **2019**, *11*, 6802−6809.
(24) Rahman, M. T.; Rana, S. S.; Salauddin, M.; Maharjan, P.; Bhatta, T. Biomechanical Energy-Driven Hybridized Generator as a Universal Portable Power Source for Smart/Wearable Electronics. *Adv. Energy Mater.* **2020**, *10*, 1903663.
(25) Jiang, T.; Pang, H.; An, J.; Lu, P.; Feng, Y.; Liang, X.; Zhong, W.; Wang, Z. L. Robust Swing-Structured Triboelectric Nanogenerator for Efficient Blue Energy Harvesting. *Adv. Energy Mater.* **2020**, *10*, 2000064.
(26) Jeong, C. K.; Hyeon, D. Y.; Hwang, G.-T.; Lee, G.-J.; Lee, M.-K.; Park, J.-J.; Park, K.-I. Nanowire-Percolated Piezoelectric Copolymer-Based Highly Transparent and Flexible Self-Powered Sensors. *J. Mater. Chem. A* **2019**, *7*, 25481−25489.
(27) Wang, Z. L.; Song, J. H. Piezoelectric Nanogenerators Based on Zinc Oxide Nanowire Arrays. *Science* **2006**, *312*, 242−246.
(28) Chou, X.; Zhu, J.; Qian, S.; Niu, X.; Qian, J.; Hou, X.; Mu, J.; Geng, W.; Cho, J.; He, J.; Xue, C. All-in-One Filler-Elastomer-Based High-Performance Stretchable Piezoelectric Nanogenerator for Kinetic Energy Harvesting and Self-Powered Motion Monitoring. *Nano Energy* **2018**, *53*, 550−558.
(29) Zi, Y. L.; Lin, L.; Wang, J.; Wang, S.; Chen, J.; Fan, X.; Yang, P. K.; Yi, F.; Wang, Z. L. Triboelectric-Pyroelectric-Piezoelectric Hybrid Cell for High-Efficiency Energy-Harvesting and Self-Powered Sensing. *Adv. Mater.* **2015**, *27*, 2340−2347.
(30) Lee, M.; Chen, C. Y.; Wang, S.; Cha, S. N.; Park, Y. J.; Kim, J. M.; Chou, L. J.; Wang, Z. L. A Hybrid Piezoelectric Structure for Wearable Nanogenerators. *Adv. Mater.* **2012**, *24*, 1759−1764.
(31) Lee, K. J.; Park, K.-I.; Kim, D. K.; Kim, S. O.; Hwang, G.-T. Flexible Nanocomposite Generator and Method for Manufacturing the Same. US 8803406 B2, 2014-08-12.
(32) Han, M.; Zhang, X. S.; Sun, X.; Meng, B.; Liu, W.; Zhang, H. Magnetic-Assisted Triboelectric Nanogenerators as Self-Powered Visualized Omnidirectional Tilt Sensing System. *Sci. Rep.* **2015**, *4*, 1−7.
(33) Hu, Y.; Yang, J.; Niu, S.; Wu, W.; Wang, Z. L. Hybridizing Triboelectrification and Electromagnetic Induction Effects for High-Efficient Mechanical Energy Harvesting. *ACS Nano* **2014**, *8*, 7442−7450.
(34) Seol, M.-L.; Han, J.-W.; Park, S.-J.; Jeon, S.-B.; Choi, Y.-K. Hybrid Energy Harvester with Simultaneous Triboelectric and Electromagnetic Generation from an Embedded Floating Oscillator in a Single Package. *Nano Energy* **2016**, *23*, 50−59.
(35) Liu, L.; Shi, Q.; Lee, C. A Novel Hybridized Blue Energy Harvester Aiming at All-Weather IoT Applications. *Nano Energy* **2020**, *76*, 105052.
(36) Yang, W.; Chen, J.; Zhu, G.; Wen, X.; Bai, P.; Su, Y.; Lin, Y.; Wang, Z. L. Harvesting Vibration Energy by a Triple-Cantilever Based Triboelectric Nanogenerator. *Nano Res.* **2013**, *6*, 880−886.
(37) Erturun, U.; Eisape, A.; West, J. E. Structures Design and Analysis of a Vibration Energy Harvester Using Push-Pull Electrostatic Conversion. *Smart Mater. Struct.* **2020**, *29*, 105018.
(38) Huang, L.; Lin, S. Z.; Xu, Z. S.; Zhou, H.; Duan, J. J.; Hu, B.; Zhou, J. Fiber-Based Energy Conversion Devices for Human-Body Energy Harvesting. *Adv. Mater.* **2020**, *32* (5), 1902034.
(39) Zi, Y. L.; Wang, J.; Wang, S.; Li, S.; Wen, Z.; Guo, H.; Wang, Z. L. Effective Energy Storage from a Triboelectric Nanogenerator. *Nat. Commun.* **2016**, *7*, 1−8.
(40) Fan, F. R.; Tian, Z. Q.; Wang, Z. L. Flexible Triboelectric Generator! *Nano Energy* **2012**, *1*, 328−334.
(41) Wu, Y. S.; Liu, Q.; Cao, J.; Li, K.; Cheng, G. G.; Zhang, Z. Q.; Ding, J. N.; Jiang, S. Y. Design and Output Performance of Vibration

https://dx.doi.org/10.1021/acsnano.0c07498
ACS Nano XXXX, XXX, XXX−XXX

Energy Harvesting Triboelectric Nanogenerator. *Wuli Xuebao* **2019**, *68*, 190201.
(42) Niu, S. M.; Liu, Y.; Wang, S. H.; Lin, L.; Zhou, Y. S.; Hu, Y. F.; Wang, Z. L. Theory of Sliding-Mode Triboelectric Nanogenerators. *Adv. Mater.* **2013**, *25*, 6184−6193.
(43) Wang, Z. L. On the First Principle Theory of Nanogenerators from Maxwell's Equations. *Nano Energy* **2020**, *68*, 104272.
(44) Nie, J.; Wang, Z.; Ren, Z.; Li, S.; Chen, X.; Wang, Z. L. Power Generation from the Interaction of a Liquid Droplet and a Liquid Membrane. *Nat. Commun.* **2019**, *10*, 1−10.
(45) Zhu, G.; Chen, J.; Zhang, T.; Jing, Q.; Wang, Z. L. Radial-Arrayed Rotary Electrification for High Performance Triboelectric Generator. *Nat. Commun.* **2014**, *5*, 1−9.
(46) Yu, A. F.; Jiang, P.; Wang, Z. L. Nanogenerator as Self-Powered Vibration Sensor. *Nano Energy* **2012**, *1*, 418−423.
(47) Han, J. H.; Bae, K. M.; Hong, S. K.; Park, H.; Kwak, J.-H.; Wang, H. S.; Joe, D. J.; Park, J. H.; Jung, Y. H.; Hur, S.; Yoo, C. D.; Lee, K. J. Machine Learning-Based Self-Powered Acoustic Sensor for Speaker Recognition. *Nano Energy* **2018**, *53*, 658−665.
(48) Wang, J.; Wang, H.; Li, X.; Zi, Y. L. Self-Powered Electrowetting Optical Switch Driven by a Triboelectric Nanogenerator for Wireless Sensing. *Nano Energy* **2019**, *66*, 104140.
(49) Xu, W.; Huang, L.-B.; Wong, M.-C.; Chen, L.; Bai, G.; Hao, J. Environmentally Friendly Hydrogel-Based Triboelectric Nanogenerators for Versatile Energy Harvesting and Self-Powered Sensors. *Adv. Energy Mater.* **2017**, *7*, 1601529.
(50) Chen, H.; Xing, C.; Li, Y.; Wang, J.; Xu, Y. Triboelectric Nanogenerators for a Macro-Scale Blue Energy Harvesting and Self-Powered Marine Environmental Monitoring System. *Sustainable Energy Fuels* **2020**, *4*, 1063−1077.
(51) Shu Fang, L.; Tsai, C. Y.; Xu, M. H.; Wu, S. W.; Lo, W. C.; Lu, Y. H.; Fuh, Y. K. Hybrid Nano-Textured Nanogenerator and Self-Powered Sensor for On-Skin Triggered Biomechanical Motions. *Nanotechnology* **2020**, *31*, 155502.
(52) Han, J. H.; Kwak, J.-H.; Joe, D. J.; Hong, S. K.; Wang, H. S.; Park, J. H.; Hur, S.; Lee, K. J. Basilar Membrane-Inspired Self-Powered Acoustic Sensor Enabled by Highly Sensitive Multi Tunable Frequency Band. *Nano Energy* **2018**, *53*, 198−205.
(53) Fu, Y.; Ouyang, H.; Davis, R. B. Effects of Electrical Properties on Vibrations *via* Electromechanical Coupling in Triboelectric Energy Harvesting. *J. Phys. D: Appl. Phys.* **2020**, *53*, 215501.
(54) Cho, S.; Yun, Y.; Jang, S.; Ra, Y.; Choi, J. H.; Hwang, H. J.; Choi, D.; Choi, D. Universal Biomechanical Energy Harvesting from Joint Movements Using a Direction-Switchable Triboelectric Nanogenerator. *Nano Energy* **2020**, *71*, 104584.
(55) Li, H.; Zhang, X.; Zhao, L.; Jiang, D.; Xu, L.; Liu, Z.; Wu, Y.; Hu, K.; Zhang, M.-R.; Wang, J.; Fan, Y.; Li, Z. A Hybrid Biofuel and Triboelectric Nanogenerator for Bioenergy Harvesting. *Nano-Micro Lett.* **2020**, *12*, 1−12.
(56) Xi, Y.; Guo, H.; Zi, Y.; Li, X.; Wang, J.; Deng, J.; Li, S.; Hu, C.; Cao, X.; Wang, Z. L. Multifunctional TENG for Blue Energy Scavenging and Self-Powered Wind-Speed Sensor. *Adv. Energy Mater.* **2017**, *7*, 1602397.
(57) Feng, L.; Liu, G.; Guo, H.; Tang, Q.; Pu, X.; Chen, J.; Wang, X.; Xi, Y.; Hu, C. Hybridized Nanogenerator Based on Honeycomb-Like Three Electrodes for Efficient Ocean Wave Energy Harvesting. *Nano Energy* **2018**, *47*, 217−223.
(58) Jiang, T.; Pang, H.; An, J.; Lu, P.; Feng, Y.; Liang, X.; Zhong, W.; Wang, Z. L. Robust Swing-Structured Triboelectric Nanogenerator for Efficient Blue Energy Harvesting. *Adv. Energy Mater.* **2020**, *10*, 2000064.
(59) Feng, Y.; Jiang, T.; Liang, X.; An, J.; Wang, Z. L. Cylindrical Triboelectric Nanogenerator Based on Swing Structure for Efficient Harvesting of Ultra-Low-Frequency Water Wave Energy. *Appl. Phys. Rev.* **2020**, *7*, 021401.
(60) Nie, J.; Chen, X.; Wang, Z. L. Electrically Responsive Materials and Devices Directly Driven by the High Voltage of Triboelectric Nanogenerators. *Adv. Funct. Mater.* **2019**, *29*, 1806351.
(61) Cheng, J.; Ding, W.; Zi, Y.; Lu, Y.; Ji, L.; Liu, F.; Wu, C.; Wang, Z. L. Triboelectric Microplasma Powered by Mechanical Stimuli. *Nat. Commun.* **2018**, *9*, 1−11.
(62) Liu, F.; Liu, Y.; Lu, Y.; Wang, Z.; Shi, Y.; Ji, L.; Cheng, J. Electrical Analysis of Triboelectric Nanogenerator for High Voltage Applications Exampled by DBD Microplasma. *Nano Energy* **2019**, *56*, 482−493.
(63) Wang, Z.; Shi, Y.; Liu, F.; Wang, H.; Liu, X.; Sun, R.; Lu, Y.; Ji, L.; Wang, Z. L.; Cheng, J. Distributed Mobile Ultraviolet Light Sources Driven by Ambient Mechanical Stimuli. *Nano Energy* **2020**, *74*, 104910.
(64) Nie, J.; Chen, X.; Wang, Z. L. Electrically Responsive Materials and Devices Directly Driven by the High Voltage of Triboelectric Nanogenerators. *Adv. Funct. Mater.* **2019**, *29*, 1806351.
(65) Xia, X.; Fu, J.; Zi, Y. A Universal Standardized Method for Output Capability Assessment of Nanogenerators. *Nat. Commun.* **2019**, *10*, 1−9.
(66) Zhu, G.; Peng, B.; Chen, J.; Jing, Q.; Wang, Z. L. Triboelectric Nanogenerators as a New Energy Technology: From Fundamentals, Devices, to Applications. *Nano Energy* **2015**, *14*, 126−138.
(67) Yang, W.; Chen, J.; Zhu, G.; Yang, J.; Bai, P.; Su, Y.; Jing, Q.; Cao, X.; Wang, Z. L. Harvesting Energy from the Natural Vibration of Human Walking. *ACS Nano* **2013**, *7*, 11317−11324.
(68) Chandrasekhar, A.; Alluri, N. R.; Vivekananthan, V.; Purusothaman, Y.; Kim, S.-J. A Sustainable Freestanding Biomechanical Energy Harvesting Smart Backpack as a Portable-Wearable Power Source. *J. Mater. Chem. C* **2017**, *5*, 1488−1493.
(69) Rome, L. C.; Flynn, L.; Goldman, E. M.; Yoo, T. D. Generating Electricity While Walking with Loads. *Science* **2005**, *309*, 1725−1728.
(70) Yuan, Y.; Liu, M.; Tai, W.-C.; Zuo, L. Design and Treadmill Test of a Broadband Energy Harvesting Backpack with a Mechanical Motion Rectifier. *J. Mech. Des.* **2018**, *140*, 085001.
(71) He, L.; Xiong, C.; Zhang, Q.; Chen, W.; Fu, C.; Lee, K. M. A Backpack Minimizing the Vertical Acceleration of the Load Improves the Economy of Human Walking. *IEEE Trans. Neural Syst. Rehabil. Eng.* **2020**, *28*, 1994−2004.
(72) Donelan, J. M.; Li, Q.; Naing, V.; Hoffer, J. A.; Weber, D. J.; Kuo, A. D. Biomechanical Energy Harvesting: Generating Electricity during Walking with Minimal User Effort. *Science* **2008**, *319*, 807−810.
(73) Rome, L. C.; Flynn, L.; Yoo, T. D. Rubber Bands Reduce the Cost of Carrying Loads. *Nature* **2006**, *444*, 1023−1024.
(74) Zou, H.; Zhang, Y.; Guo, L.; Wang, P.; He, X.; Dai, G.; Zheng, H.; Chen, C.; Wang, A. C.; Xu, C.; Wang, Z. L. Quantifying the Triboelectric Series. *Nat. Commun.* **2019**, *10*, 1−9.
(75) Zhang, X.; Chen, L. F.; Jiang, Y.; Lim, W. C.; Soh, S. Rationalizing the Triboelectric Series of Polymers. *Chem. Mater.* **2019**, *31*, 1473−1478.

https://dx.doi.org/10.1021/acsnano.0c07498
ACS Nano XXXX, XXX, XXX−XXX